Enrichment Using Antibody-Coated Microfluidic Chambers in Shear Flow: Model Mixtures of Human Lymphocytes

Aaron Sin, Shashi K. Murthy, Alexander Revzin, Ronald G. Tompkins, Mehmet Toner

Surgical Services and Center of Engineering in Medicine, Massachusetts General Hospital, Harvard Medical School, and Shriners Hospital for Children, Boston, Massachusetts 02114; telephone: (617) 371-4883; fax: (617) 371-4950; e-mail: mtoner@hms.harvard.edu

Received 26 October 2004; accepted 1 April 2005

Published online 21 July 2005 in Wiley InterScience (www.interscience.wiley.com). DOI: 10.1002/bit.20556

Abstract: Isolation of phenotypically-pure cell subpopulations from heterogeneous cell mixtures such as blood is a difficult yet fundamentally important task. Current techniques such as fluorescent activated cell sorting (FACS) and magnetic-activated cell sorting (MACS) require pre-incubation with antibodies which lead to processing times of at least 15–60 min. In this study, we explored the use of antibody-coated microfluidic chambers to negative deplete undesired cell types, thus obtaining an enriched cell subpopulation at the outlet. We used human lymphocyte cell lines, MOLT-3 and Raji, as a model system to examine the dynamic cell binding behavior on antibody coated surfaces under shear flow. Shear stress ranging between 0.75 and 1.0 dyn/cm^2 was found to provide most efficient separation. Cell adhesion was shown to follow pseudo-first order kinetics, and an anti-CD19 coated (Raji-depletion) device with ~2.6 min residence time was demonstrated to produce 100% pure MOLT-3 cells from 50-50 MOLT-3/Raji mixture. We have developed a mathematical model of the separation device based on the experimentally determined kinetic parameters that can be extended to design future separation modules for other cell mixtures. We conclude that we can design microfluidic devices that exploits the kinetics of dynamic cell adhesion to antibody coated surfaces to provide enriched cell subpopulations within minutes of total processing time.

Keywords: cell affinity chromatography; microfluidic devices; blood cell separation; immobilized antibodies; dynamic cell adhesion

INTRODUCTION

There is an ever-increasing need for isolation of phenotypically-pure cell subpopulations from a heterogeneous mixture of cells, for example, blood in both clinical and research settings. In the clinical side, identification and quantification of specific blood cell subpopulations can be very helpful in disease diagnostics, for example CD4/CD8 ratios in AIDS. On the other hand, use of pure cells help reduce variations among experiments and thus expedite scientific discovery.

Fluorescent activated cell sorting (FACS) is currently one of the most prevalent techniques for affinity-based isolation. Cell mixtures are fluorescently labeled using specific dyes or antibodies to surface antigens, and then sorted one by one based on light scattering and fluorescent properties. This technique results in highly pure cell populations that can be sorted by multiple parameters, at the expense of costly equipment and limited throughput (~10^7 cells/h) (Putnam et al., 2003; Thiel et al., 1998). Magnetic-activated cell sorting (MACS) is also used in the isolation of cells by a single parameter using antibody-coated magnetic beads. Since labeled cells are processed in parallel, high cell numbers can be processed within a short time (10^8–10^9 cells/h) (Thiel et al., 1998). Recent improvements including continuous sorting (Haik et al., 1999; McCloskey et al., 2003; Zborowski et al., 1999) and multiple parameter sorting (Partington et al., 1999; Thiel et al., 1998) make magnetic sorting a favorable alternative to FACS.

The common thread among FACS, MACS, and other similar techniques such as density perturbation (Patel et al., 1995), is the requirement of pre-processing incubation with various forms of antibody tags (fluorescent, beads, etc.). The number of parameters accessible to separation is thus limited to the availability of distinct tags, such as excitation and emission bands of fluorophores and density, size, and magnetophoretic mobility of beads. Separation efficiency depends both on the antibody binding capacity of cells (McCloskey et al., 2003), which is inherent to the specific cell surface marker, and the yield of antibody tag binding during pre-processing, which is a function of processing conditions, such as time, mixing, and concentration (Patel and Rickwood, 1995). This pre-incubation step increases the amount of time needed for separation (15–60 min) and

Correspondence to: Mehmet Toner
Contract grant sponsors: National Institutes of Health (BioMEMS Resource Center); Croucher Foundation Fellowship

Contract grant number: P41 EB002503

This article includes supplementary material available via the Internet at http:www.interscience.wiley.com/jpages/0006-3592/suppmat.

necessitates the use of skilled technicians. Microscale versions of FACS (Fu et al., 2002) and MACS (Berger et al., 2001) exist but both require the pre-incubation step.

One strategy is to eliminate tagging using technologies such as counterflow centrifugal elutriation (CCE) (Bauer, 1999; Donaldson et al., 1997), which separates based on size and density. While this type of technology is powerful in separating cell mixtures with significant difference in sizes as reviewed by Bauer (1999), it does not provide enough resolution to distinguish among blood cell or stem cell mixtures. Similarly, while dielectrophoretic fractionation techniques can be useful to purify leukocytes from whole blood (Auerswald and Knapp, 2003; Yang et al., 1999), it would not be very effective in isolating $CD4^+$ T cells from other lymphocytes.

By immobilizing the antibodies directly onto surfaces, cell affinity chromatography (CAC) systems removes the need for pre-incubation while conserving the resolution and specificity of separation (Mandrusov et al., 1995; Putnam et al., 2003). Yields and purity can be comparable to FACS and MACS with reasonable throughput (10^8–10^9 cells/h) (Putnam et al., 2003). To increase active surface area per unit volume, most macroscopic CAC systems adopt a packed bed design, giving rise to residence times in the order of 1–2 h (Putnam et al., 2003; Ujam et al., 2003). Long residence time was also required in a hollow fiber design (Mandrusov et al., 1995). This lengthy processing time is again undesirable especially when further experimentation or analysis is necessary.

In this study, we examine the feasibility of using microfluidic devices to enrich blood cell subpopulations based on the CAC concept. Because of their length scales, microfluidic devices provide the high surface area to volume ratios required in traditional CACs while processing times can be kept short by running many parallel devices. Using MOLT-3 and Raji cell lines as model systems, we explore the use of dynamic cell adhesion on antibody-coated microfluidic chambers to enrich lymphocyte mixtures. In dynamic cell adhesion, cells attach to the surfaces directly from the flow stream, as opposed to static cell adhesion where the cells are allowed to settle and adhere to the surfaces at zero flow before being detached by shear forces. We aim to adsorb or negatively deplete one cell type from the flow stream onto the corresponding antibody-coated surface (anti-CD5 for MOLT-3 capture and anti-CD19 for Raji capture) and produce an enriched population of the other cell type in the outlet stream. By modeling the kinetics of this dynamic cell adhesion behavior, we demonstrate cell subpopulation enrichment can be obtained within minutes of processing, while removing the need for antibody pre-incubation.

EXPERIMENTAL

Materials

3-mercaptopropyl trimethoxysilane was obtained from Gelest (Morrisville, PA). 200 proof ethanol, glass slides (35×60 mm, no.1), tissue culture flasks, serological pipets, and microslide field finders were purchased from Fisher Scientific (Fair Lawn, NJ). Four-inch diameter (100 mm) soda lime glass wafers were obtained from Eric Scientific (Portsmouth, NH). For chamber fabrication, SU-8 photoresist and developer were obtained from MicroChem (Newton, MA); silicone elastomer and curing agent were obtained from Dow Corning (Midland, MI). Phosphate buffered saline (PBS) $1\times$ and RPMI-1640 cell culture medium were obtained from Mediatech (Herndon, VA). Fetal bovine serum (FBS) and 0.5M ethylenediaminetetraacetic acid (EDTA) were purchased from Gibco (Grand Island, NY). Dimethyl sulfoxide (DMSO), sodium azide, lyophilized bovine serum album (BSA), and a glove bag for handling the moisture-sensitive silane were obtained from Aldrich Chemical Co. (Milwaukee, WI). The coupling agent GMBS (*N*-y-maleimidobutyryloxy succinimide ester) and fluorescein-conjugated NeutrAvidin were obtained from Pierce Biotechnology (Rockford, IL). Each 50 mg batch of GMBS was dissolved in 0.5 mL of DMSO. Biotinylated mouse anti-human anti-CD5 and anti-CD19, were purchased from Serotec Antibodies (Raleigh, NC). Human mature naive B-lymphocyte (Raji) and immature T-lymphoblast (MOLT-3) cell lines were purchased from American Type Culture Collection (Manassas, VA). The lyophilized FITC labeled NeutrAvidin was restored with distilled water as recommended by the manufacturer. Cell tracker dyes green 5-chromethylfluorescein diacetate (CMFDA) and orange 5-(and-6)-(((4-chloromethyl)-benzoyl) amino)tetramethyl-rhodamine (CMTMR) were obtained from Molecular Probes (Eugene, OR).

Chamber Designs

Two microfluidic devices are used in this work. The Hele-Shaw flow chamber design (see Fig. 1A), where the wall shear stress decreases linearly in the axial direction, was described in Usami et al. (1993). The fabricated flow chambers were 57 ± 1 μm in height with inlet width and total length being 5 and 50 mm, respectively. The parallel flow chamber design (see Fig. 1B), which provides a constant shear stress throughout, consists of eight radially distributed parallel serpentine flow channels with dimensions 1 mm $\times$ 160 mm $\times$ (70 ± 2 μm) ($w \times l \times h$) each. Multiple parallel channels were used to increase total surface area for separation and more importantly to minimize syringe pump oscillations which are especially evident at low flow rates. The entire parallel device fits on a 4 inches (100 mm) diameter glass wafer.

Chamber Fabrication

Microfluidic flow chambers were assembled at the Bio-MEMS Resource Center at MGH. A high-resolution transparency (CAD/Art Services, Inc., Poway, CA) was generated from an Auto-CAD file created in-house. This transparency was used to generate a negative master. Briefly, a silicon wafer was coated with SU-8 to a desired thickness.

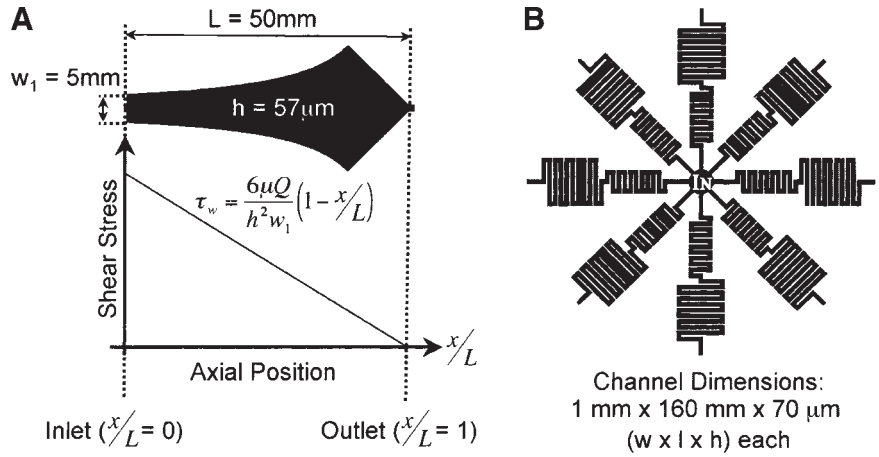

Figure 1. Schematics of the two microfluidic chambers used in this study: (**A**) Hele-Shaw flow chamber and its shear stress profile, as well as the (**B**) parallel flow chamber.

With the transparency overlaid, the wafer was then exposed to 365 nm, 11 mW/cm^2 UV light from a Q2001 mask aligner (Quintel Co., San Jose, CA). Unexposed SU-8 was then removed using developer. Feature height was verified using a Dektak surface profiler (Veeco Instruments, Santa Barbara, CA). Silicone elastomer and curing agent were mixed (10:1 ratio) and poured on top of the wafers and allowed to cure overnight in an oven at 65°C. Holes for the inlet and outlet ports on the poly(dimethylsiloxane) (PDMS) replicas were punched out with a blunt-nosed needle. PDMS replicas and glass substrates were cleaned with an oxygen plasma (100 mW, 1% oxygen, 30 s) in a PX-250 plasma chamber (March Instruments, Concord, MA) and then immediately placed in contact to bond the surfaces irreversibly. Glass cover slips were used in for the construction for Hele-Shaw flow chambers, while glass wafers were used as substrates for the parallel flow devices. Surface modification was carried out immediately after bonding.

Surface Modification

Chambers were flushed with a 4% (v/v) silane solution in ethanol (solution prepared under a nitrogen atmosphere in a glove bag) and allowed to react at room temperature for 30 min. Unreacted silane was removed by flushing with ethanol. The chambers were then flushed with 1 μM GMBS solution in ethanol and allowed to react for 15 min. After flushing with ethanol, the chambers were flushed with a 1 μg/mL Neutravidin solution in PBS and stored overnight in a refrigerator. The chambers were flushed with PBS and used in flow experiments or modified further as follows. The antibody stocks were diluted with a solution of PBS containing 1% (w/v) BSA and 0.09% (w/v) sodium azide to a concentration of 10 μg/mL and flowed through the chambers. After a 15-min period, the chambers were flushed with PBS to remove unattached antibody. We have previously determined the antibody surface concentration to be ~60 molecules/μm^2 for both anti-CD5 and anti-CD19 (Murthy et al., 2004).

Flow Experiments

Raji and MOLT-3 cells were cultured in 150-cm^2 tissue culture flasks at 37°C in a humidified atmosphere with 5% CO_2. MOLT-3 cells are human immature T-lymphoblasts that express CD5 but not CD19. Raji cells are human mature B-lymphocyte and they express CD19 but not CD5. The cells were incubated in RPMI-1640 supplemented with 10% FBS, 200 U/mL penicillin. For use in experiment, the cell suspension was centrifuged at 150*g* for 5 min and then resuspended in PBS to remove dead cells and cell debris. After centrifuging again 150*g* for 5 min, the cells were resuspended in PBS with 1 mM EDTA to obtain a concentration of approximately 1×10^6 cells/mL. Cell concentrations were estimated using a hemacytometer. For experiments with MOLT-3/Raji cell mixtures, the cells were stained with green and orange cell tracker dyes, respectively. The cell suspension drawn from the culture flask was centrifuged at 800*g* for 5 min, resuspended in 10 mL phenol-red free RPMI-1640 containing 4 mM of cell tracker dye and incubated for 30 min at 37°C. Centrifugation and resuspension in PBS/EDTA were the performed as described above.

As mentioned before, two different devices were used for experiments. The Hele-Shaw devices were used to understand dynamic cell attachment behavior at different shear rates, since multiple shear rates can be obtained in each flow chamber without changing inlet flow rates. The parallel flow devices were used for time course and enrichment experiments, where the operating shear stress was determined by examining the Hele-Shaw experimental data.

In experiments using the Hele-Shaw device, 0.5 mL of cell suspension was introduced at the desired flow rate (usually between 30 and 50 μL/min) to antibody-coated Hele-Shaw chambers (anti-CD5 or anti-CD19) using a Harvard Apparatus PHD 2000 syringe pump (Holliston, MA). The volume of cell suspension was chosen such that cell adhesion on the surfaces reaches a pseudo steady state. For the experiment with cell mixtures, a cell suspension that consisted of with 1.2:1.0 (or 55%:45%) MOLT-3 to Raji cells at a total

concentration of 1.0×10^6 cells/mL was used. For experiments with pure cells, we used cell suspensions at initial concentrations ranging from 0.8 to 1.3×10^6 cells/mL. Immediately after the cell suspension has been delivered, unbound cells were removed by flushing PBS through the chamber at the same flow rate as the cell deposition step. The switch between cell suspension and PBS was done as quickly as possible to maintain non-zero flow in the chamber at all times. Care must also be taken not to introduce sudden jerks in the fluid flow during the switch so that the attached cells are not dislodged. Cell adhesion was measured by placing a field finder under the chambers and counting cells at select points along the flow chamber central axis using a Nikon Eclipse TE2000 inverted microscope (Nikon, Japan). For each point, the number of cells adhered at three 1 mm^2 squares near the central axis were manually counted, and averaged. Results from multiple experiments were normalized to 1.0×10^6 cells/mL by dividing with initial cell concentration. Cell mixtures were examined and photographed using a SPOT digital camera (Diagnostic Instruments, Inc., Burlingame, CA) attached to the Nikon microscope.

In time course experiments, a randomly selected location on the antibody-coated parallel flow device (anti-CD5 or anti-CD19) was monitored using an 8-bit color CCD camera at the Nikon inverted microscope and recorded on VCR (Sony SVO-9500 MD, Sony, Japan). The parallel flow devices were operated at 35 μL/min (0.84 ± 0.02 dyn/cm^2) for Raji cell capture and 30 μL/min (0.79 ± 0.02 dyn/cm^2) for MOLT-3 cell capture. The number of cells attached at each 3 s time point was manually counted on playback. Cell drifting velocities were also obtained from these experiments using Metamorph image analysis software, where the distances traveled between frames were measured and divided by the lapsed time. At least 100 cell velocities from each experiments were obtained, and the mean and standard deviation of the traveling velocity distributions were calculated.

In the enrichment experiment, we used a cell suspension at the total concentration of 2.3×10^6 cells/mL with 1.0:1.3 (or 43%:57%) MOLT-3 to Raji cells. This cell suspension was introduced to an anti-CD5 coated device and an anti-CD19 coated device at 30 μL/min (0.79 ± 0.02 dyn/cm^2) and 35 μL/min (0.84 ± 0.02 dyn/cm^2), respectively. The proportion of fluorescently labeled MOLT-3 and Raji cells at the outlet of the parallel flow device were determined by direct observation through the Nikon microscope.

THEORETICAL

Microfluidic Chambers

Hele-Shaw flow occurs in flow chambers where the third dimension (height) is very small compared to the other two dimensions. The Hele-Shaw chamber takes advantage of the equipotential lines in Hele-Shaw flow to create a chamber with linear shear gradient (Usami et al., 1993). The wall shear stress (τ_w) profile for the Hele-Shaw devices along axial positions (x) can be expressed in Eq. 1, where Q is the volumetric flow rate, μ is the viscosity of water, and h, w_1, and L are the height, inlet width, and total length of the flow chamber, respectively.

$$\tau_w = \frac{6\mu Q}{h^2 w_1}\left(1 - \frac{x}{L}\right) \tag{1}$$

Also, at the centerline of the Hele-Shaw chamber and in parallel flow channels, the fluid velocity at a particular vertical position (z) is shown in Eq. 2) (Usami et al., 1993). This rearranges to give Equation 3, which estimates the vertical distance between the center of a cell in motion and the chamber floor, if the drifting velocity can be measured.

$$v = \frac{\tau_w}{\mu}\frac{z(h-z)}{h} \tag{2}$$

$$z = \frac{1}{2}\left[h - \sqrt{h^2 - \frac{2v\mu h}{\tau_w}}\right] \tag{3}$$

Cell Adhesion Kinetics

The kinetics of cell adhesion to antibody-coated surfaces can be rationalized as a pseudo-first order binding dependent on the number of available discrete sites on the surface, $s(t)$, assuming excess supply of cells (see Eq. 4). The resultant number of bound cells, $b(t)$ is expressed in Equation 4. The parameter s_0 represents the total number of sites available on a surface.

$$\begin{aligned} &\text{cell} + \text{site} \xrightarrow{ks(t)} \text{bound} \\ &\frac{ds(t)}{dt} = -\frac{db(t)}{dt} = -ks(t) \\ &s(t) = s_0 e^{-kt} \\ &b(t) = s_0(1 - e^{-kt}) \end{aligned} \tag{4}$$

Sometimes bound cells detach from the surface either by shear flow or collision by another cell in suspension. We can update the cell binding model with the reverse reaction (see Eq. 5). This modification results in the same fundamental form as Equation 4 with apparent rate constant, k_{app} and apparent saturation constant $s_{0\ app}$, which are basically k and s_0 modified by combinations of the forward and reverse rate constants (k_{on} and k_{off}).

Separation Device Modeling

$$\begin{aligned} &\text{cell} + \text{site} \underset{k_{off}b(t)}{\overset{k_{on}s(t)}{\rightleftharpoons}} \text{bound} \\ &\frac{ds(t)}{dt} = -\frac{db(t)}{dt} = -k_{on}s(t) + k_{off}b(t) \\ &s(t) = s_0\left[\frac{k_{off}}{k_{on}+k_{off}} + \frac{k_{on}}{k_{on}+k_{off}}e^{-(k_{on}+k_{off})t}\right] \\ &b(t) = s_{0\cdot app}(1 - e^{-k_{app}t}) \\ &\text{where } s_{0app} = s_0\frac{k_{on}}{k_{on}+k_{off}}; \quad k_{app} = k_{on} + k_{off} \end{aligned} \tag{5}$$

A model of the parallel plate separation device can be constructed as a plug flow reactor using reaction rates as derived in Equation 4 with modified by surface area to volume ratio, $A = 1/h = 1/(70\ \mu m)$, and a pure time delay function, since axial and transverse dispersions of cells are negligible in microfluidic environments (see Eq. 6). We assume that undesired interactions can be made negligible by operating device at higher shear rate, therefore any other cell types that are not specifically captured are ignored in this model. Note that because the binding kinetics was a pseudo-zeroth order with respect to cell concentration in the flow, the resultant expression predicts negative $\mathscr{C}$'s (non-dimensionalized flow stream cell concentration) which should then be set to zero. The variable τ represents the residence time or the "time position" (position normalized by linear velocity, x/v). The Heaviside function in the final expression, $\mathscr{H}(t-\tau)$, signifies the time delay in plug flow reactors, where the concentration should be zero at all τ until at ($t = \tau$ when the cell plug arrives at that particular location.

$$\frac{\partial c}{\partial t} + v\frac{\partial c}{\partial x} = -ksA$$

$$\text{where } s = s_0 e^{-k(t-\tau)}; \quad \mathscr{C} = \frac{c}{c_0}; \quad \tau = \frac{x}{v}$$

$$\frac{\partial \mathscr{C}}{\partial t} + \frac{\partial \mathscr{C}}{\partial \tau} = -\frac{ks_0 A}{c_0} e^{-k(t-\tau)}$$

$$\mathscr{C} = \mathscr{H}(t-\tau)\left[1 - \frac{ks_0 A}{c_0}\tau e^{-k(t-\tau)}\right] \qquad (6)$$

Finally, we introduce a parameter, θ, the capture window, which is the period of time when the outlet concentration of the captured cell is zero or when the opposite cell is 100% pure. This capture window, which can be obtained by setting $\mathscr{C} = 0$ in Equation 6, is shown in Equation 7 as a function of the natural log of the total residence time ($\ln \tau_0$).

$$\theta = \frac{1}{k}\ln\left(\frac{ks_0 A}{c_0}\tau_0\right) \qquad (7)$$

RESULTS

Dynamic Cell Adhesion at Pseudo Steady State

We first sought to understand the pseudo steady state dynamic cell adhesion behavior at varying shear stresses, where cells from constant flow stream adheres to the bottom surface of the flow chamber. This behavior is in contrast to static cell adhesion where cells are introduced to a surface, allowed to attach for a period of time without flow and then detached by shear force. To achieve this goal, we performed an experiment using the Hele-Shaw device with a 55:45 MOLT-3 to Raji cell mixture. Figure 2 shows fluorescence microscopy images of adhered MOLT-3 cells and Raji cells on anti-CD5 and anti-CD19 surfaces at different axial positions of the Hele-Shaw chamber, corresponding to shear stresses of 0.60 dyn/cm^2 and 1.0 dyn/cm^2. Note the larger number of Raji (red-stained) cells adhered to anti-CD19 compared to the number of MOLT-3 (green-stained) cells adhered to anti-CD5 at the corresponding shear

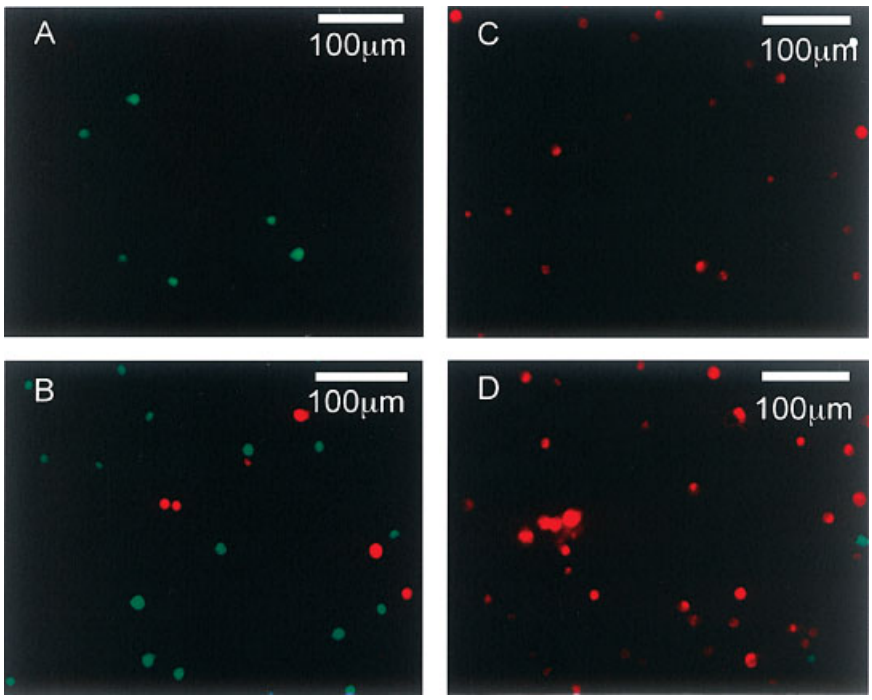

Figure 2. Images showing fluorescently labeled MOLT-3 (green) and Raji (red) cells adhered to different shear stress regions in the antibody-coated Hele-Shaw chambers: (**A**) anti-CD5, 1.0 dyn/cm^2; (**B**) anti-CD5, 0.6 dyn/cm^2; (**C**) anti-CD19, 1.0 dyn/cm^2; (**D**) anti-CD19, 0.6 dyn/cm^2. The chambers were infused with 0.5 mL of 1.0×10^6 cells/mL cell suspension with 1.2:1.0 MOLT-3 to Raji.

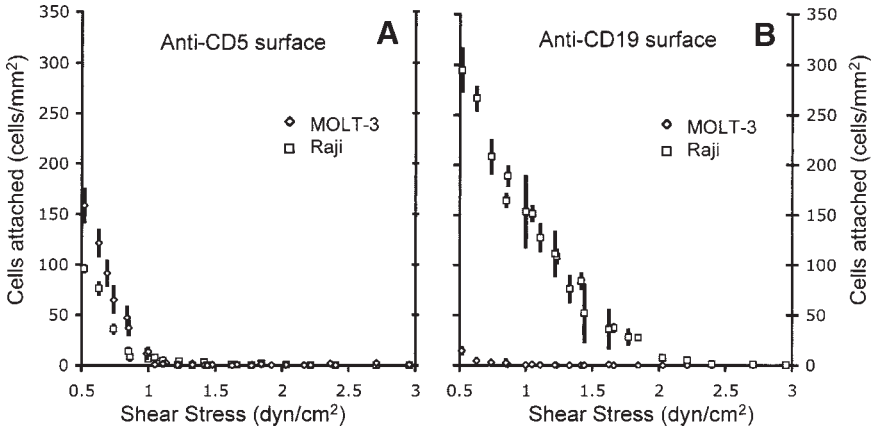

Figure 3. Dynamic cell adhesion of MOLT-3 cells (◇) and Raji (□) on CD5 (left) and CD19 (surfaces). These graphs combine data points from at least three experiments spanning different shear stress ranges, with error bars representing standard deviations in measurements within each experiment. All experiments were performed by introducing 0.5 mL of MOLT-3 or Raji cell suspension at $\sim 1 \times 10^6$ cells/mL into antibody-coated Hele-Shaw chambers at flow rates between 30 and 50 μL/min. The resultant cell attached per mm^2 data are then normalized by simple division to a cell concentration of 1.0×10^6 cells/mL.

rates. We also observed a higher adhesion of Raji cells on anti-CD5 surfaces comparing to MOLT-3 on anti-CD19 surfaces.

We conducted the experiments using the Hele-Shaw device with pure suspensions of Raji and MOLT-3 cells to further dissect this cell adhesion phenomenon. Figure 3 shows the number of cells adhered to anti-CD5 and anti-CD19 surfaces as a function of shear stress. As seen in Figure 3, the number of cells adhered increases at lower shear stresses. Raji cells adhere almost twice as much on anti-CD19 surfaces as MOLT-3 cells on anti-CD5 surfaces at low shear stresses. The shear at which Raji cells starts adhering to anti-CD19 surface ($\sim$2 dyn/cm^2) is also higher than that of MOLT-3 cells on anti-CD5 surface ($\sim$1 dyn/cm^2). Adhesion of MOLT-3 cells on anti-CD19 surfaces remains relatively low throughout the range of shear stress examined. However, adhesion of Raji cells on anti-CD5 surfaces starts increasing below 0.8 dyn/cm^2. The number of Raji cells adhered to anti-CD5 surfaces is about one-third of the number of Raji cells adhered to anti-CD19 surfaces at 0.5 dyn/cm^2. The data in Figure 3 support the observation in Figure 2.

Figure 3 can now be used as a "phase-diagram" for separation between MOLT-3 and Raji cells on anti-CD5 and anti-CD19 surfaces, respectively. Our goal is to adsorb or negatively deplete one cell type from the flow stream onto the corresponding antibody coated surface (anti-CD5 for MOLT-3 capture and anti-CD19 for Raji capture), resulting in an enriched population of the other cell type in the outlet stream. We would introduce cell suspensions into an antibody-coated device at a constant shear stress, thus achieving cell separation based on the difference in cell adhesion numbers between the two cells. Data from Figure 3 indicate that we can operate the separation devices at shear stresses ranging between 0.75 and 1.0 dyn/cm^2, where we can negatively deplete the one cell type with relatively high efficiency, while suffering close to zero loss in the cells of interest. Based on this information, we performed subsequent experiment in parallel flow devices operating at constant shear stresses: The MOLT-3 capture devices (anti-CD5 coated) were operated at 0.79 dyn/cm^2, while the Raji capture devices were operated at 0.84 dyn/cm^2.

Dynamic Cell Adhesion Kinetics

We then tested our pseudo-first order kinetics hypothesis (see Eq. 4). Time course experiments using anti-CD19 coated parallel flow devices were performed with Raji cell suspensions at different initial concentrations. The number of bound cells as a function of time, $b(t)$, was experimentally measured and fitted to Equation 4, as shown in Figure 4. The fitted parameters: pseudo-first order rate constant, k, and

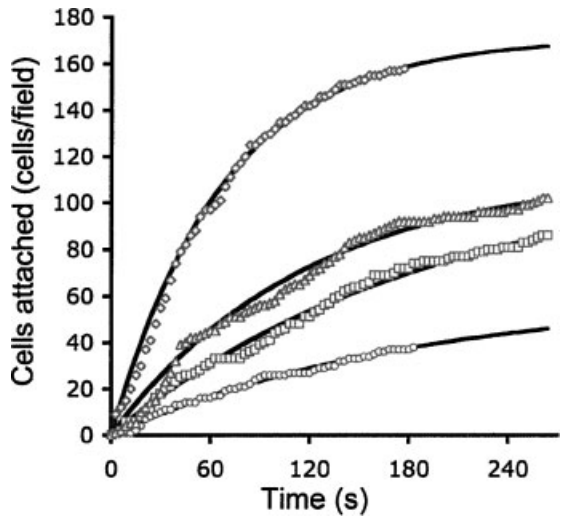

Figure 4. The kinetics of Raji cell adhesion to anti-CD19 coated parallel flow device. Number of cells attached in each random microscope field (0.88 mm^2) is plotted against time for different initial feed concentrations: 0.4 (○), 0.75 (□), 1.15 (◇), and 1.55 (△) $\times 10^6$ cells/mL. These data points are fitted to a pseudo-first order kinetic model (Eq. 4). The resultant least-square fit is shown here as solid lines, with the fitted parameters shown in Table I.

Table I. Fitted parameters to the cell binding kinetic model for different initial cell concentrations.

	Concentration (10^6 cells/mL)	Fitted s_0 (cells/field[a])	Normalized s_0 (cells/mm^2)	1° coefficient k (10^{-2}/s)
Raji	0.4	60	68	0.55
	0.75	114	130	0.53
	1.15	171	194	1.5
	1.55	113	126	0.86
	2.2	61	69	0.36
	4.3	36	41	0.42
MOLT-3	0.85	53	60	0.20
	1.55	56	64	0.23

[a]Microscope field = 0.88 mm^2.

saturation number of sites, s_0 are listed in Table I. Experiments were also performed with MOLT-3 cells in anti-CD5 coated parallel flow devices. Results indicated that MOLT-3 cell adhesion follows similar, but slower saturation kinetics (see Supplemental Fig. 1) and the corresponding fitted kinetic parameters are also shown in Table I. An interesting result to note is that s_0/c_0 is a constant (0.17/mm) for the Raji initial concentrations of 0.4, 0.75, and 1.15×10^6 cells/mL. At higher Raji concentrations, both s_0 and k decrease with concentration.

From the videos of these time course experiments, Raji traveling velocities were also measured, with the means and standard deviations summarized in Table II. The vertical distance between the cell center and the chamber floor was estimated using Equation 3. Since both MOLT-3 and Raji cells were around 6–8 μm in diameter, the percentage of cells with cell center closer than 4 μm from the bottom surface (cell velocity < 635 μm/s) were also presented in Table II. From this data, we see that the percentage of Raji cells traveling in close proximity to the channel bottom surface increases with cell concentration.

Separation Device Experiments and Modeling

After studying both the pseudo steady state (Hele-Shaw experiments) and kinetic dynamic cell adhesion behaviors (time course experiments), we used the parallel channel device to separate MOLT-3 and Raji cell mixtures. An anti-CD5 coated device and an anti-CD19 coated device were used to enrich Raji cells and MOLT-3 cells from a 43:57 MOLT-3/Raji cell suspension respectively. It was observed that at the outlet of the anti-CD19 coated device (Raji depletion), 100% pure MOLT-3 population eluted for ~1.5 min.

Table II. Drifting velocities of Raji cells in attachment experiments for different initial cell concentrations.

Concentration (10^6 cells/mL)	Velocity $\bar{v} \pm \sigma_v$(μm/s)	Vertical position $\bar{z} \pm \sigma_z$(μm)	$v < 635$ μm/s or $z < 4$ μm
0.75	829 ± 167	5.3 ± 0.05	29%
1.15	842 ± 161	5.4 ± 0.05	27%
2.2	851 ± 216	5.5 ± 0.06	33%
4.3	797 ± 268	5.1 ± 0.09	44%

After this initial 1.5 min, the proportion of Raji cells continued to increase for the next ~3 min until the outlet cell composition approached that of the inlet cell suspension. In the anti-CD5 device (MOLT-3 depletion), the MOLT-3 proportion only reduced to about half of the inlet concentration (~75% Raji), which was expected due to the lower affinity of MOLT-3 cells (see Fig. 3). Examination of the cell adhesion surfaces revealed that 35 ± 7 MOLT-3 cells/mm^2 and 5 ± 4 Raji cells/mm^2 adhered to the anti-CD5 coated surface, while 249 ± 14 Raji cells/mm^2 and <1 MOLT-3 cells/mm^2 attached to the anti-CD19 coated surface (see Fig. 5). The standard deviation among at least three measurements is listed as uncertainties. The number of cells attached was again in agreement with Figure 3. Finally, the throughputs of the anti-CD5 and anti-CD19 enrichment experiments can be obtained by multiplying the input cell concentration (2.3×10^6 cells/mL) to the flow rates (30 and 35 μL/min), which translate to 4.1×10^6 cells/h and 4.8×10^6 cells/h, respectively.

We now turn to the mathematical model to rationalize our separation device results and to enable future designs. Calculated using the model derived in Equation 6, Figure 6

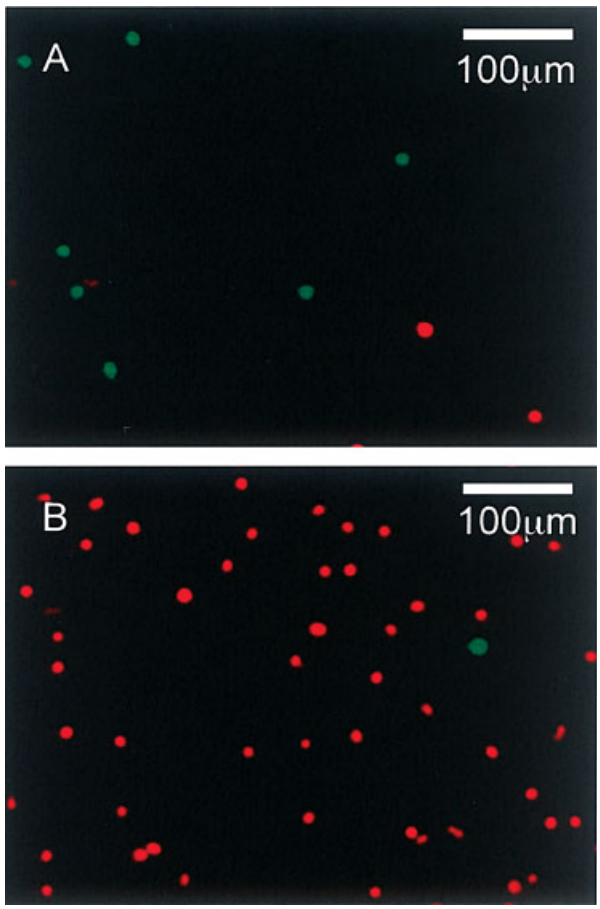

Figure 5. Images showing fluorescently labeled MOLT-3 (green) and Raji (red) cells captured at the surfaces of (**A**) anti-CD5 coated and (**B**) anti-CD19 coated parallel flow devices. The anti-CD5 and anti-CD19 devices were operated at 0.79 ± 0.02 dyn/cm^2 (30 μL/min) and 0.89 ± 0.02 dyn/cm^2 (35 μL/min), respectively. A cell suspension at 2.3×10^6 cells/mL cell suspension with 1.0:1.3 MOLT-3 to Raji was used for both experiments.

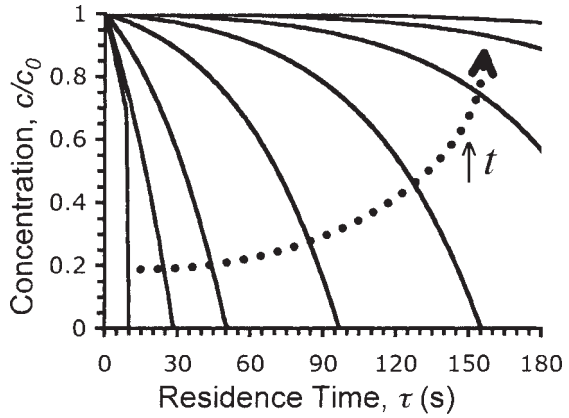

Figure 6. Modeled behavior of flow stream cell concentration within the separation device with respect to residence time (τ) or "time positions." The concentration profile at different real time points (left to right): $t = 10$, 30, 60, 90, 180, 270, 360, 450 s are shown as solid curves. This model was evaluated with k = 0.015/s and $s_0/c_0 = 0.168$/mm.

shows non-dimensionalized concentration $\mathscr{C}$ plotted against the time positions or residence times τ at different real time t, modeling Raji cells depletion at initial feed concentration c_0 being 1.15×10^6 cells/mL with wall shear stress at 0.84 dyn/cm^2 (see Table I) where k = 0.015/s and $s_0/c_0 = 0.17$/mm. At a very short time ($t = 10$ s), cell concentration decays in the separation device as cells are being absorbed relatively quickly by the empty substrate, up to the front of the cell plug, where concentration of cells drops to zero. As more cells are being introduced, the cell front progresses through the parallel flow device, with the slope of cell concentration over residence time curve $(d\mathscr{C}/d\tau)$ becoming more gradual and the surfaces of the separation device getting saturated. Eventually ($t = 450$ s in Fig. 6), the concentration remains at its inlet concentration for the majority of the device and only reduces slightly towards the end of the device.

One can then envision building a longer device such that more total number of cells can be depleted from the flow without saturating the separation device. Figure 7 shows the concentration of cells eluding from devices of different length or total residence time, τ_0, as a function of real time delayed by the total residence time of the reactor, $t-\tau_0$, for the same Raji depletion experiment ($c_0 = 1.15 \times 10^6$ cells/mL). As to be expected, the concentration of eluding Raji cells starts at low level and gradually increase to $\mathscr{C} = 1$ or initial feed concentration. The curves shift to the right for longer devices (higher τ_0). A feature to note in Figure 7 is the capture window: the length of time when the concentration of eluding Raji cells is zero or the opposite cell (MOLT-3 in this case) is 100% pure (see Eq. 7). More particularly, the model would predict that our anti-CD19 separation device with $\tau_0 = 153$ s provide a capture window of 114 s for a Raji depletion experiment with $c_0 = 1.3 \times 10^6$, which is close to the ~1.5 min observed experimentally as described previously.

Figure 8 shows the behavior of capture window, θ, as a function of device residence time, τ_0 for different k and s_0/c_0 values. Firstly, since θ is a function of ln τ_0, the marginal gain in capture window decreases at longer device lengths $(\text{or } d^2\theta/d\tau_0^2 < 0)$. Keeping k constant, the capture window increases with increasing s_0/c_0 since more cells can be depleted with same length of device, τ_0. Less efficient depletion (smaller k) results in longer capture window if the device is long enough, or shorter capture window or inadequate separation for small τ_0.

DISCUSSION

Our overall goal is to study the feasibility of using microfluidic devices to enrich cell populations based on the CAC concept. Using a MOLT-3 and Raji cells as our model system, we explored the use of dynamic cell adhesion to antibody coated surface in shear flow as a separation driving force. In our experiments, we first mapped the pseudo steady state cell adhesion behavior for MOLT-3 and Raji cells on anti-CD5 and anti-CD19 surfaces at different shear stresses

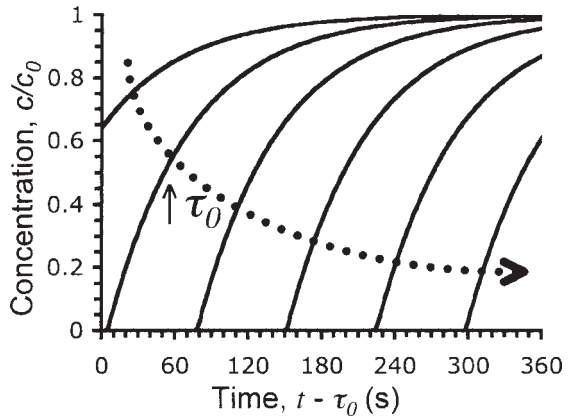

Figure 7. Modeled behavior of outlet flow stream cell concentration of the separation device with respect to real time ($t-\tau$). The concentration profile for different device lengths or residence times (left to right): $\tau_0 = 10$, 30, 90, 270, 810, 2,430 s are shown as solid curves. This model was evaluated with k = 0.015/s and $s_0/c_0 = 0.168$/mm.

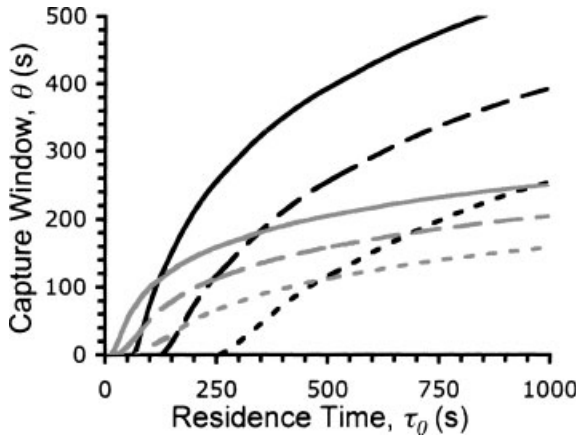

Figure 8. Modeled behavior of capture window with respect to device residence time (τ_0). The effect of different parameters were investigated: k = 0.005/s (black) and 0.015/s (gray) with $s_0/c_0 = 0.20$/mm (solid lines), 0.10/mm (dashed lines), and 0.05/mm (dotted lines).

using Hele-Shaw devices. From this data, we chose operating shear stresses for the anti-CD5 and anti-CD19 parallel flow devices for subsequent experiments, where we studied the cell adhesion kinetics. We also used the parallel flow devices to enrich Raji and MOLT-3 populations from almost 50-50 mixtures. Finally, we explored a mathematical model built upon the experimental determined kinetic data to understand the enrichment experiment results. In this section, we will discuss the observed cell adhesion saturation kinetics, particularly the validity of the measured parameters. We will also examine the impact of various parameters in the mathematical model on separation device design.

As shown in Figure 3 and Table I, dynamic MOLT-3 cell adhesion to anti-CD5 surfaces is much slower and lower in numbers than Raji cell adhesion on anti-CD19 surfaces. This low binding phenomenon can potentially be contributed to low antibody-antigen binding affinity for the lot of anti-CD5 antibodies used, or low number of CD5 antigens surface expressed per MOLT-3 cell, or both. This low binding efficiency can be remedied either by choosing another antigen target (e.g., CD2 or CD3) or testing different anti-CD5 clones. The relatively high Raji adhesion on anti-CD5 surfaces may be due to the expression of semi-specific complement activated membrane receptors such as IgM and CR2 (CD21) on Raji cells (Hess et al., 2000), while traces of complement molecules might have remained from FBS used for cell culture. Regardless of the reason, study of dynamic cell adhesion as a function of shear stress provides a way of enriching cell populations based on affinity to specific antibodies while reducing or eliminating the effect of undesired adhesions, a problem that is ubiquitous in immune cell handling.

In Table I, the saturation constant (s_0) is shown to increase linearly at low cell concentrations ($\leq 1.15 \times 10^6$ cells/mL), but decrease at higher cell concentration. We believe that the decreasing trend at higher concentrations is caused partially by increased interactions between an adhered cell and a cell in the flow stream, particularly since the percentage of cells that traveling close to the channel bottom increase with concentration. It was observed in the time course experiments that cells tend to travel near the chamber floor and stop abruptly when captured by antibody, or flow around an adhered cell. Minimal cell rolling interactions with the surface was observed in experiments with cell concentrations of $\leq 1.15 \times 10^6$ cells/mL. At higher cell concentrations ($>1.15 \times 10^6$ cells/mL), more ''stop-and-go'' cell interactions were observed, where a cell would approach the surface, stop briefly for <1 s and continue drifting. In addition, more detachment events occur at higher cell concentration, which was not observed at low cell concentrations.

We can account for these detachment events with a reversible binding model (see Eq. 5), which results in the same fundamental form as Equation 4 with apparent rate constant, k_{app} and apparent saturation constant $s_{0\ app}$ being k and s_0 modified by combinations of the forward and reverse rate constants (k_{on} and k_{off}). This modification by the reverse rate constant helps explain the decreasing trend in fitted $s_{0\ app}$ at high concentrations. The kinetic rate constants themselves, k_{on} and k_{off}, are complex functions of factors such as cell sedimentation rate at different cell concentrations, cell receptor density and cell viability which are not included in the simple kinetic model.

While the saturation phenomenon can be explained by simple first-order kinetic modeling, the relatively low saturation number of cells may appear counter-intuitive. Particularly, 200 Raji cells/mm^2 only occupies 1% of the available surface area. Similar behavior has been reported previously (Mandrusov et al., 1995), where about 200 lymphocytes/mm^2 adhered to antibody coated cellophane membrane at 40/s shear rate (0.4 dyn/cm^2). One theory could be that the antibody coverage is non-uniform. However, atomic force microscopy data (Murthy et al., 2004) indicate that the antibody coverage is about 60 molecules/μm^2, which is uniform from a cell's perspective. Moreover, the fact that the adhesion increases sharply with decreased shear rate (see Fig. 3) and Mandrusov et al. (1995) indicates much higher capabilities of the antibody-coated surfaces for cell adsorption.

Another possible explanation is that the hydrodynamic shear forces prevented cells from approaching the substrate, as documented in Cantat and Misbah (1999); Segré and Silberberg (1961); Williams et al. (1992). However, we operated our microfluidic devices at a Reynold's number of 0.1 and shear stresses less than 1 dyn/cm^2, which are below the thresholds at which shear lifting of particles occur (Cantat and Misbah, 1999; Segré and Silberberg, 1961). Moreover, we observed that the cells are introduced within 10 μm from the subtrate at the vertically installed inlet. Therefore, the cell-substrate collision frequency should be fairly high, as described in Hodges and Jensen (2002); Zhang and Neelamegham (2002).

We believe that the saturation number of cells per unit area can be related to wall shear stress or drifting velocity. We have measured the average Raji traveling velocities at 0.89 dyn/cm^2 wall shear stress to be around 800 μm/s (see Table II), which corresponds to the bottom of a cell being 1–2 μm from the antibody-coated floor. This relatively high velocity shows that a majority of the cells were drifting with the fluid flow as opposed to engaging in rolling interaction with the antibody-coated surface. As we have observed, drifting cells either flow around adhered cells on the surface or stop abruptly when they move close enough to the wall and captured by antibodies. Homotypic aggregation (cell–cell interaction) effects are negligible in our case because of the addition of EDTA in the cell suspension (Simon and Goldman, 2002; Ujam et al., 2003). The addition of EDTA was necessary to remove cell aggregates in the flow stream. Consider that it takes O(10 ms) for a cell from 500 nm above the floor to approach an adhesive surface (Hodges and Jensen, 2002), and that the receptor-ligand binding is a stochastic event with efficiency in the order of 10% (Simon and Goldman, 2002), it is then reasonable to assume a period of O(0.1 s) for a cell to transition from the ''drifting'' to the ''capture'' phase. Moreover, if a cell encounters an adhered

cell during this transition period, this process starts all over again after the drifting cell avoids the adhered cell. The length of this transition period would then dictate a characteristic distance of ~100–400 μm between two adhered Raji cell in the same horizontal streamline, which can be observed in Figure 5B. Similarly, the saturation number of cells for MOLT-3 is lower because of the possibly lower binding probability and thus longer period for a MOLT-3 cell to transition to the capture phase (see Fig. 5A).

In Figure 4, small deviations from the cell binding kinetic model can be observed at short times ($t < 30$ s). This deviation can be contributed to the pseudo-first order assumption made based on excess supply of cells in the flow stream. Since the time course measurement were performed at around the midpoint of the parallel channels due to practical concerns, much of the cells have been depleted from the flow stream, as predicted in Figure 6. Fortunately, the cell supply soon becomes abundant, when surfaces at the beginning of the device become saturated. Since the least-square fit was computed based on data from the entire experiment of more than 150 s, we can neglect the resultant uncertainty in the fitted parameters for use in the model of the separation device.

This pseudo-first order assumption does become problematic in the complete cell separation device model when predicting capture windows. When flow stream cell concentration ($\mathscr{C}$) approaches zero, the binding efficiency can be lower than what the pseudo-first order model is predicting, especially when the surfaces at the end of the device is near saturation. This lower binding efficiency leads to a slightly shorter capture window than predicted, which can help explain the difference between the experimentally observed ~1.5 min and predicted 114 s capture window for the Raji depletion experiment discussed earlier. The exact model can be obtained assuming second order kinetics ($\text{rate}_{\text{depletion}} = -\text{k}c(t)s(t)$), which makes fitting to experimental data more challenging. On the other hand, it was difficult to accurately measure the capture window by observing fluorescent labeled cells microscopically when they travel in excess of 800 μm/s in the device.

Finally, the $\ln \tau_0$ dependency of the capture window (Fig. 7) means that parallel operation of many relatively short separation device would be more efficient than few very long ones. In the case of Raji depletion, devices with total residence times between 100 and 200 s would appear to offer the best compromise of separation and processing time, providing capture windows between of 100 and 150 s. In other words, this anti-CD19 coated device can provide pure MOLT-3 populations from a binary mixture in less than 6 min. Depletion of MOLT-3 cells from the binary mixture using an anti-CD5 device is more difficult due to the low binding affinity of MOLT-3 and relatively high binding level of Raji, but a 10 min long device can still provide a 1 min capture window. On the other hand, because of the slow binding kinetics ($\text{k} = 0.02$), very long capture windows can theoretically be obtained ($\theta = 10$ min for $\tau_0 = 33$ min) with this anti-CD5 device.

We can therefore operate 20–50 anti-CD19 devices in parallel to yield similar processing throughput as FACS and MACS technologies. The prototype anti-CD19 devices ($\tau_0 = \sim 150$ s) fit comfortably on a 4 inches (100 mm) diameter glass wafer; 50 of these devices will occupy less than 6 feet^2 (5,000 cm^2) footprint if assembled in a single layer. Devices with much longer residence times (such as the proposed anti-CD5 device) can be fabricated on the same footprint (or smaller) by stacking multiple layers of PDMS devices.

To sum up, the nature of microfluidic channels help make our enrichment devices more efficient than their macroscopic counterparts, since they can be operated at similar shear stress ranges with lower Reynold's number, thereby increasing cell-substrate collisions. By modeling the cell adhesion kinetics, we were also able to take advantage of faster kinetics of cell adhesion when compared to the ''equilibrium mode'' in the pre-incubation steps necessary for FACS and MACS techniques.

CONCLUSIONS

We studied the feasibility of microfluidic enrichment of model lymphocyte cell line mixtures through negative depletion of undesired cells. We used MOLT-3 and Raji cell lines as model systems, a $CD5^+CD19^-$ human T-lymphoblast and $CD5^-CD19^+$ human B-lymphocyte, respectively. We obtained the dynamic cell adhesion profiles of both cells on anti-CD5 and anti-CD19 surfaces at pseudo steady state. We found that at shear stresses around 0.75 to 1.0 dyn/cm^2, we can capture cells based on affinity to antibody coated surfaces while reducing or eliminating undesired binding by the cell of interest. We also verified that the dynamic cell adhesion of Raji and MOLT-3 follows a pseudo-first order kinetic model. From an almost 50-50 mixture of MOLT-3 and Raji cells, we were also able to obtain 100% pure MOLT-3 cells with an anti-CD19 coated device with ~2.6 min residence time. An anti-CD5 coated device with a ~3.0 min residence time produced ~75% Raji cells from the same cell mixture.

Using experimentally determined kinetic parameters, we created a mathematical model to describe the operation of a microfluidic enrichment device. The prediction from this model matched well with experimental separation results, and showed that cell enrichment from MOLT-3/Raji cell mixtures can be performed within minutes of processing time. Particularly, we found that the capture window, defined as the period of time at the outlet where 100% depletion was obtained, is dependent on the natural log of the device residence time. This finding indicates that an optimal device design would consist of multiple relatively short channels operating in parallel opposed to long channels to provide cell enrichment with short overall processing times. We can also operate 20–50 devices in parallel to obtain similar throughput as FACS and MACS technologies.

In summary, we have demonstrated the possibility of using dynamic cell attachment to antibody-coated microfluidic

chambers in shear flow to enrich mixtures of MOLT-3 and Raji cells. More importantly, we have developed a mathematical model, which can be extended to design separation modules for other cell mixtures, such as human peripheral blood leukocytes. A protocol for experimentally determining key design parameters was also established. By taking advantage of the kinetics of dynamic cell adhesion, antibody-coated microfluidic devices can be designed to enrich cell subpopulations with only minutes of processing time, completely eliminating the need for time intensive antibody pre-incubation step.

A.S. thanks the Croucher Foundation Fellowship for financial support. Technical assistance from Octavio Hurtado was greatly appreciated.

References

Auerswald J, Knapp HF. 2003. Quantitative assessment of dielectrophoresis as a microfluidic retention and separation technique for beads and human blood erythrocytes. Microelectronic Eng 67–68:869–886.

Bauer J. 1999. Advances in cell separation: Recent developments in counterflow centrifugal elutration and continuous flow cell separation. J Chromatography B 722:55–69.

Berger M, Castelino J, Huang R, Shah M, Austin RH. 2001. Design of a microfabrication magnetic cell separator. Electrophoresis 22:3883–3892.

Cantat I, Misbah C. 1999. Lift force and dynamical unbinding of adhering vesicles under shear flow. Phys Rev Lett 83:880–883.

Donaldson KL, McShea A, Wahl AF. 1997. Separation by counterflow centrifugal elutration and analysis of T- and B- lymphocytic cell lines in progressive stages of cell division cycle. J Immunol Methods 203:25–33.

Fu AY, Chou H-P, Spence C, Arnold FH, Quake SR. 2002. An integrated microfabricated cell sorter. Anal Chem 74:2451–2457.

Haik Y, Vinay P, Chen C-J. 1999. Development of magnetic device for cell separation. J Magnetism Magn Mater 194:254–261.

Hess MW, Schwendinger MG, Eskelinen E-L, Pfaller K, Pavelka M, Dierich MP, Prodinger WM. 2000. Tracing uptake of C3dg-conjugated antigen into B cells via complement receptor type 2 (CR2, 2D21). Blood 95:2267–2623.

Hodges SR, Jensen OE. 2002. Spreading and peeling dynamics in a model of cell adhesion. J Fluid Mech 460:381–409.

Mandrusov E, Houng A, Klein E, Leonard EF. 1995. Membrane-based cell affinity chromatography to retieve viable cells. Biotechnol Prog 11: 208–213.

McCloskey KE, Moore LR, Hoyos M, Rodriguez A, Chalmers JJ, Zborowski M. 2003. Magnetophoretic cell sorting is a function of antibody binding capacity. Biotechnol Prog 19:889–907.

Murthy SK, Sin A, Tompkins RG, Toner M. 2004. Effect of flow and surface conditions on human lymphocyte isolation using microfluidic chambers. Langmuir 20:11649–11655.

Partington KM, Jenkinson EJ, Anderson G. 1999. A novel method of cell separation based on dual parameter immunomagnetic cell selection. J Immunol Methods 223:195–204.

Patel D, Rickwood D. 1995. Optimization of conditions for specific binding of antibody-coated beads to cells. J Immunol Methods 184:71–80.

Patel D, Rubbi CP, Rickwood D. 1995. Separation of T and B lymphocytes from human peripheral blood mononuclear cells using density perturbation methods. Clinica Chimica Acta 240:187–193.

Putnam DD, Namasivayam V, Burns MA. 2003. Cell affinity separations using magnetically stabilized fluidized beds: Erythrocyte subpopulation fractionation utilizing a lectin-magnetite support. Biotechnol Bioeng 81:650–655.

Segré G, Silberberg A. 1961. Radial poiseuille flow of suspensions. Nature 189:209.

Simon SI, Goldman HL. 2002. Leukocyte adhesion dynamics in shear flow. Ann Biomed Eng 30:315–332.

Thiel A, Scheffold A, Radbruch A. 1998. Immunomagnetic cell sorting—pushing the limits. Immunotechnology 4:89–96.

Ujam LB, Clemmitt RH, Clarke SA, Brooke RA, Rushton N, Chase HA. 2003. Isolation of monocytes from human peripheral blood using immuno-affinity expanded-bed adsorption. Biotechnol Bioeng 83:554–566.

Usami S, Chen H-H, Zhao Y, Chien S, Skalak R. 1993. Design and construction of a linear shear stress flow chamber. Ann Biomed Eng 21:77–83.

Williams PS, Koch T, Giddings JC. 1992. Characterization of near-wall hydrodynamic lift forces using sedimentation field-flow fractation. Chem Eng Comm 111:121–147.

Yang J, Huang Y, Wang X-B, Becker FF, Gascoyne PRC. 1999. Cell separation on micro-fabricated electrotrodes using dielectrophoretic/gravitation field-flow fractionation. Anal Chem 71:911–918.

Zborowski M, Sun L, Moore LR, Williams PS, Chalmers JJ. 1999. Continuous cell separation using novel magnetic quadruple flow sorter. J Magnetism Magn Mater 194:224–230.

Zhang Y, Neelamegham S. 2002. Estimating the efficiency of cell capture and arrest in flow chambers: Study of neutrophil binding via E-selectin and ICAM-1. Biophys J 83:1934–1952.